Electronic Structure of the α-(BEDT-TTF)2MHg(XCN)4 (M = Tl, K, NH4; X = S, Se) and Related Phases. Synthesis and Crystal Structure of the New Stable Organic Metal α-(BEDT-TTF)2TlHg(Se1-xSxCN)4 (x = 0.125)

R. Rousseau, M.-L. Doublet, E. Canadell, R. Shibaeva, S. Khasanov, L. Rozenberg, N. Kushch, E. Yagubskii

J. Phys. I France 6 (1996) 1527–1553 DECEMBER 1996, PAGE 1527

Electronic Structure of the α-(BEDT-TTF)$_2$MHg(XCN)$_4$ (M = Tl, K, NH$_4$; X = S, Se) and Related Phases. Synthesis and Crystal Structure of the New Stable Organic Metal α-(BEDT-TTF)$_2$TlHg(Se$_{1-x}$S$_x$CN)$_4$ (x = 0.125)

R. Rousseau ([1]), M.-L. Doublet ([2]), E. Canadell ([1,2,*]), R.P. Shibaeva ([3,*]), S.S. Khasanov ([3]), L.P. Rozenberg ([3]), N.D. Kushch ([4]) and E.B. Yagubskii ([4,*])

([1]) Institut de Ciència de Materials de Barcelona (CSIC), Campus de la UAB, 08193 Bellaterra, Spain

([2]) Laboratoire de Structure et Dynamique des Systèmes Moléculaires et Solides, Université de Montpellier II, 34095 Montpellier Cedex, France

([3]) Institut of Solid State Physics, Russian Academy of Sciences, Chernogolovka MD, 142432 Russia

([4]) Institut of Chemical Physics at Chernogolovka, Russian Academy of Sciences, Chernogolovka MD, 142432 Russia

(Received 8 April 1996, accepted 1 July 1996)

PACS.71.25.Rv – Polymers and organic compounds
PACS.71.30.+h – Metal-insulator transitions and other electronic transitions
PACS.74.70.Kn – Organic superconductors

Abstract. — The synthesis, crystal structure, conductivity and electronic band structure of the new molecular metal α-(BEDT-TTF)$_2$TlHg(Se$_{1-x}$S$_x$CN)$_4$ ($x = 0.125$) are reported. α-(BEDT-TTF)$_2$TlHg(Se$_{1-x}$S$_x$CN)$_4$ ($x = 0.125$) is isostructural with all other members of the family of α-(BEDT-TTF)$_2$MHg(XCN)$_4$ salts and is a stable metal down to very low temperatures. A general study of the electronic structure of all structurally characterized α-(BEDT-TTF)$_2$MHg(XCN)$_4$ salts as well as α-(BEDT-TTF)$_2$I$_3$, α-(BEDT-TTF)$_2$IBr$_2$ and α-(BEDT-TTF)$_4$PtBr$_6$ is also reported. Different aspects related to the electronic structure of these salts like the stability of the metallic state and the nature of the Fermi surface are discussed and correlated with the details of their crystal structures. The origin of the different dimensionality of the carriers for the α-(BEDT-TTF)$_2$MHg(XCN)$_4$ salts (*i.e.*, 1D electrons but 2D holes) , the metal to insulator transition in α-(BEDT-TTF)$_2$I$_3$ and the semiconducting behavior of α-(BEDT-TTF)$_2$IBr$_2$ and α-(BEDT-TTF)$_4$PtBr$_6$ are also discussed.

1. Introduction

The α-(BEDT-TTF)$_2$MHg(XCN)$_4$ (M = K, Rb, Tl; X = S, Se) phases [1–4] have provided a seemingly endless series of intriguing results. All of these salts are two-dimensional metals down to the lowest temperatures and display a remarkable diversity in their physical properties.

(*) Authors for correspondence (e-mail: canadell@zas.qf.ub.es, shibaeva@issp.ac.ru, yagubski@icp.ac.ru)

For instance, the K(S), Rb(S) and Tl(S) salts have a resistivity anomaly at 8 K, 12 K and 10 K respectively [5–7], which is believed to originate from a density wave instability of the Fermi surface [8]. In contrast, the NH_4(S) and the Tl(Se) salts do not exhibit such anomaly [9, 11]. However, whereas the first of these two salts becomes superconducting at about 1 K and ambient pressure [9], the second stays metallic down to very low temperatures and does not enter into the superconducting state [9,10]. Pressure suppresses the low temperature resistivity anomaly of the K(S), Rb(S) and Tl(S) salts [11, 12] as well as the superconductivity of the NH_4(S) salt [13].

The diversity in physical properties is most intriguing if we take into account the great similarity in the crystal [1–4] and electronic structures [2, 14] of all these phases. The Fermi surface of these salts exhibits both one-dimensional (1D) and two-dimensional (2D) portions with identical area. Extensive magnetoresistance studies have shown that the size of the 2D portion of the Fermi surface is approximately 16% of the first Brillouin zone for all of the α-(BEDT-TTF)$_2$MHg(XCN)$_4$ (M = K, Rb, Tl; X = S, Se) salts [7, 12, 15–20]. Studies of the pressure dependence of the Fermi surface have shown that the area of the closed portion increases by approximately 21% under 1 kbar for both the K(S) [12] and Tl(Se) [21] salts, *i.e.*, one salt exhibiting the low temperature resistivity anomaly and another that does not. On the basis of these and similar results it is not expected that the Fermi surfaces of the different α-(BEDT-TTF)$_2$MHg(XCN)$_4$ phases are significantly different. In fact, the calculated Fermi surfaces for the K(S) and NH_4(S) salts seem to substantiate this expectation [2, 14]. However, the diversity in the low temperature physical behavior makes difficult to understand why this should be so. Very recently, the synthesis of the K(Se) salt has further increased the list of puzzling questions about these phases. It has been reported [22] that, according to magnetoresistance experiments, the size of the closed part is again 16% of the first Brillouin zone and that the calculated Fermi surface is practically indistinguishable from that of the K(S) salt. Yet, the K(Se) salt does not exhibit the low temperature resistivity anomaly of the K(S) salt.

The large number of magnetoresistance studies concerning these phases have thus led to a wealth of information about their Fermi surfaces. However, it has been difficult to integrate all these pieces of information into a general scenario which can successfully rationalize the low temperature behavior of the different α-(BEDT-TTF)$_2$MHg(XCN)$_4$ phases. Another elusive aspect has been the correlation between the details of the crystal structure and the Fermi surfaces. Although it seems to be a currently accepted idea that there are no fundamental differences among the α-(BEDT-TTF)$_2$MHg(XCN)$_4$ crystal structures, there are some indications that this is only partially correct. For instance, it has been recently reported [4] that, judging from the central C = C bond lengths, there are two different types of BEDT-TTF donors in the Tl(Se) salt but just one in the Tl(S), NH_4(S) and K(S) salts. Does this fact have some role in the peculiar behavior of the Tl(Se) salt, *i.e.*, no resistivity anomaly and no superconductivity? However, the K(Se) salt is reported [22] to have the same physical behavior and yet it has also been reported to have the same Fermi surface than the K(S) salt, which has only one type of BEDT-TTF [2].

It is clear from this short overview that we are still far from a satisfying understanding of the electronic structure of the α-(BEDT-TTF)$_2$MHg(XCN)$_4$ phases. Since the Tl(S) and Tl(Se) salts display quite a different physical behavior, we thought it would be interesting to try the synthesis of mixed Tl(S/Se) salts. In this paper we report the synthesis, crystal structure determination and conductivity of the mixed salt α-(BEDT-TTF)$_2$TlHg(Se$_{0.875}$S$_{0.125}$CN)$_4$. We also report on the band structure and Fermi surface of this new organic metal as well as on those of all other α-(BEDT-TTF)$_2$MHg(XCN)$_4$ salts whose crystal structures have, to the best of our knowledge, been reported in the literature. We also compare these results with those for

phases like α-(BEDT-TTF)$_2$I$_3$ [23–25], α-(BEDT-TTF)$_2$IBr$_2$ [26] and α-(BEDT-TTF)$_4$PtBr$_6$ [27] which, despite the close structural relationship with the α-(BEDT-TTF)$_2$MHg(XCN)$_4$ salts, exhibit definitely different physical behaviors [28–30].

2. Experimental

2.1. SYNTHESIS. — A family of α-(BEDT-TTF)$_2$MHg(XCN)$_4$ salts with mixed (SCN) and (SeCN) ligands in the anion layer could be obtained by electrochemical oxidation of BEDT-TTF using various solutions (1,2-dichloroethane, benzonitrile) and different combinations of the initial salts as electrolytes: [TlSCN + Hg(SeCN)$_2$], [TlSeCN + Hg(SCN)$_2$]. It turned out that the composition of such mixed compounds depends on both the solvent nature and the thio- or selenocyane salts of Tl and Hg used. Three different synthetic methods were used.

2.1.1. Method 1. — Plate-like crystals were obtained by electrochemical oxidation of BEDT-TTF (2×10^{-3} mol/l) on a Pt anode under galvanostatic regime ($I = 0.4$ μA) at constant temperature (20 °C). The solvent was 1,2-dichloroethane with addition of a 10% volume of absolute ethanol. The electrolyte was prepared by dissolution of 18-crown-6 ether (5×10^{-3} mol/l), TlSCN (10^{-2} mol/l), and Hg(SeCN) (5×10^{-3} mol/l) in the above mentioned solvent in an electrochemical cell. A local X-ray microprobe analysis (LRMA) indicated that the crystals are (BEDT-TTF)$_2$TlHg(Se$_{0.675}$S$_{0.325}$CN)$_4$. However, crystals with another stoichiometry were also found. Consequently, the composition of the single crystal from this synthesis was studied through a full X-ray crystal structure analysis and found to be (BEDT-TTF)$_2$TlHg(Se$_{0\ 875}$S$_{0.125}$CN)$_4$. The differences in composition may be connected with nonhomogeneity of the compound and inaccuracy of the LRMA analysis.

2.1.2. Method 2. — The conditions of the BEDT-TTF electrocrystalization were similar to those of method 1 except that benzonitrile was used instead of 1,2-dichloroethane. Three types of crystals were prepared simultaneously: plates, needles and spear-like. The plate-like crystals were found to be isostructural to the α-(BEDT-TTF)$_2$TlHg(XCN)$_4$ (X = S, Se) salts [3, 4, 7, 10, 11]. The needle and spear-like crystals were not. The composition of the former ones was determined by LRMA and found to be (BEDT-TTF)$_2$TlHg(Se$_{0.550}$S$_{0.450}$CN)$_4$. The replacement of TlSCN and Hg(SeCN) by TlSeCN and Hg(SCN), respectively, in benzonitrile (*Method 3*) led to the preparation of only plate-like crystals with stoichiometry (BEDT-TTF)$_2$TlHg(Se$_{0.775}$S$_{0\ 225}$CN)$_4$ according to LRMA.

2.2. X-RAY ANALYSIS. — The intensities of 4033 independent reflections with $I > 3\sigma(I)$ were collected on an Enraf-Nonius CAD-4F diffractometer using graphite monochromatic MoK$_\alpha$ radiation in the region of $\sin\theta/\lambda < 0.594$ by the method of $\theta/2\theta$ scans. The crystal structure was solved by a direct method and then refined by a least-squares procedure in the anisotropic/isotropic (for the H-atoms) approximation to $R = 0.058$. The AREN programs were used. The composition of the anion was determinated by the refinement of the occupancy factors for Se and S atoms in the corresponding positions of the anion layer. The final coordinates of non-hydrogen atoms and their thermal parameters are listed in Table I. The coordinates of hydrogen atoms are given in Table II.

2.3. BAND STRUCTURE CALCULATIONS. — The full tight-binding band structure calculations are based upon the effective one-electron Hamiltonian of the extended Hückel method [31]. The off-diagonal matrix elements of the Hamiltonian were calculated according to the modified Wolfsberg-Helmholz formula [32]. All valence electrons were explicitly taken into account in the calculations. The basis set consisted of double-ζ Slater type orbitals for C and S and single-ζ

Table I. — *Atomic coordinates and equivalent thermal parameters* B_{eq} *(Å²) for non-hydrogen atoms of* α-$(BEDT\text{-}TTF)_2TlHg(Se_{0.875}S_{0.125}CN)_4$.

Atom	x/a	y/b	z/c	B_{eq}
S1	0.4748 (4)	0.5906 (1)	0.3865 (5)	3.23
S2	0.5544 (4)	0.7342 (2)	0.4629 (5)	3.50
S3	0.8094 (4)	0.6902 (1)	0.2298 (5)	3.15
S4	0.6827 (4)	0.5562 (1)	0.1835 (5)	3.11
S5	0.5470 (4)	0.4049 (1)	0.0935 (5)	3.13
S6	0.4508 (4)	0.2639 (2)	0.0080 (5)	3.17
S7	0.2105 (4)	0.3102 (1)	0.2594 (5)	3.39
S8	0.3465 (4)	0.4425 (1)	0.3040 (5)	3.38
C1	0.5414 (15)	0.5313 (7)	0.2612 (19)	2.85
C2	0.5863 (15)	0.6546 (6)	0.3596 (18)	2.54
C3	0.7145 (14)	0.7770 (6)	0.4571 (18)	2.44
C4	0.7609 (18)	0.7733 (8)	0.3187 (21)	3.25
C5	0.6823 (14)	0.6399 (7)	0.2740 (19)	2.62
C6	0.4829 (17)	0.4658 (8)	0.2202 (21)	3.55
C7	0.4297 (14)	0.3434 (7)	0.1129 (18)	2.31
C8	0.3009 (15)	0.2169 (6)	0.0386 (18)	2.40
C9	0.2700 (18)	0.2288 (8)	0.1901 (21)	3.31
C10	0.3395 (14)	0.3594 (7)	0.2097 (17)	2.34
S9	0.1731 (4)	0.5560 (1)	0.6121 (5)	3.42
S10	0.3088 (4)	0.6876 (2)	0.6909 (5)	3.71
S11	0.0459 (4)	0.7377 (2)	0.5205 (5)	3.44
S12	−0.0451 (4)	0.5946 (1)	0.4564 (5)	3.29
C11	0.0272 (16)	0.5310 (8)	0.5145 (21)	3.25
C12	0.1730 (17)	0.6405 (8)	0.6035 (19)	3.13
C13	0.2782 (19)	0.7713 (8)	0.6761 (23)	4.26
C14	0.1282 (16)	0.7837 (7)	0.6753 (21)	3.30
C15	0.0765 (15)	0.6569 (6)	0.5328 (18)	2.46
S13	0.1674 (4)	0.5558 (1)	0.1226 (5)	3.42
S14	0.2967 (4)	0.6889 (2)	0.2168 (5)	3.43
S15	0.0517 (4)	0.7367 (2)	0.0141 (5)	3.57
S16	−0.0345 (4)	0.5939 (1)	−0.0544 (5)	3.36
C16	0.0280 (15)	0.5307 (7)	0.0111 (20)	2.97
C17	0.1697 (14)	0.6406 (6)	0.1158 (17)	2.20
C18	0.2494 (19)	0.7708 (8)	0.2145 (22)	3.88
C19	0.2063 (17)	0.7807 (8)	0.0809 (22)	3.47
C20	0.0771 (14)	0.6564 (7)	0.0345 (19)	2.77
Tl	0.2561 (0)	0.0258 (0)	0.2616 (0)	3.79
Hg	0.7499 (0)	−0.0062 (0)	0.2514 (0)	3.03
Se	0.5266 (1)	−0.0818 (0)	0.2324 (2)	3.51
Se, S	0.7336 (2)	0.0670 (1)	0.0695 (3)	3.80 (0.75Se+0.25S)
Se	0.9554 (1)	−0.0799 (0)	0.1895 (2)	3.67
Se, S	0.7822 (2)	0.0745 (1)	0.4953 (2)	2.72 (0.75Se+0.25S)
C21	0.5325 (15)	−0.0868 (9)	0.4069 (25)	3.08
C22	0.5611 (20)	0.0793 (9)	0.0924 (21)	3.71
C23	0.9428 (16)	−0.0847 (8)	0.0151 (23)	2.41
C24	0.9610 (20)	0.0837 (8)	0.4874 (21)	3.88
N1	0.5346 (15)	−0.0866 (8)	0.5217 (23)	4.32
N2	0.4480 (19)	0.0913 (10)	0.1069 (24)	6.32
N3	0.9377 (17)	−0.0886 (9)	−0.0953 (24)	4.41
N4	1.0781 (16)	0.0916 (8)	0.4862 (20)	4.99

Table II. — *Atomic coordinates of the hydrogen atoms of* α-$(BEDT\text{-}TTF)_2TlHg(Se_{0.875}S_{0.125}CN)_4$.

Atom	x/a	y/b	z/c
H31	0.764	0.760	0.509
H32	0.695	0.827	0.524
H41	0.687	0.786	0.253
H42	0.851	0.800	0.319
H81	0.317	0.175	−0.007
H82	0.229	0.225	−0.009
H91	0.197	0.201	0.196
H92	0.345	0.227	0.227
H131	0.286	0.774	0.577
H132	0.322	0.801	0.722
H141	0.125	0.820	0.665
H142	0.081	0.770	0.747
H181	0.340	0.799	0.250
H182	0.164	0.786	0.269
H191	0.178	0.817	0.057
H192	0.266	0.759	0.004

Table III. — *Unit cell parameters of* α-$(BEDT\text{-}TTF)_2TlHg(XCN)_4$ *with* $X = S$, *Se and* $(Se_{0.875}S_{0\ 125})$.

Parameter	Se	$Se_{0.875}S_{0\ 125}$	S
a (Å)	10.105 (1)	10.102 (1)	10.051 (2)
b (Å)	20.793 (3)	20.754 (4)	20.549 (4)
c (Å)	10.043 (1)	10.014 (1)	9.934 (2)
α (°)	103.51 (1)	103.57 (1)	103.63 (1)
β (°)	90.53 (1)	90.52 (1)	90.48 (1)
γ (°)	93.27 (1)	93.28 (1)	93.27 (1)
V (Å^3)	2047.9	2037	1990

Slater type orbitals for H. The exponents, contraction coefficients and atomic parameters used for the calculations were taken from previous work [33]. The model extended Hückel tight-binding band structure calculations are based upon the transfer integrals calculated using the dimer splitting approximation [34] and the same exponents and parameters employed in the full calculations.

3. Crystal Structures and Physical Properties of the α-(BEDT-TTF)$_2$TlHg(XCN)$_4$ (X = S, Se and Se$_{1-x}$S$_x$) Salts

The unit cell parameters of α-(BEDT-TTF)$_2$TlHg(Se$_{0.875}$S$_{0.125}$CN)$_4$ are listed in Table III together with those of the Tl(Se) [4] and Tl(S) [3] salts. As can be seen from this Table, α-(BEDT-TTF)$_2$TlHg(Se$_{0\ 875}$S$_{0\ 125}$CN)$_4$ is isostructural with the family of the α-(BEDT-TTF)$_2$MHg(XCN)$_4$ charge transfer salts. The projection of the crystal structure along the c-axis is shown in Figure 1. It contains conducting cation-radical layers of BEDT-TTF alternating along the b-axis with the insulating thick polymeric anion sheets. There are three independent donor molecules. One BEDT-TTF molecule (I) occupies the general position, and the other two (II and III) are located at inversion centers. The geometry of these molecules is shown in Figure 2. All molecules have the same eclipsed conformation of the ethylene groups without orientational disorder. However, the bond length distributions in molecules I-III differ noticeably. For example, the length of the central C = C bond in molecule I is 1.42(2) Å, which is close to the length of the same bond in the cation-radical (BEDT-TTF)$^+$. However, in molecules II and III is 1.34(2) and 1.33(2) Å respectively, in close agreement with the length of this bond in the neutral donor (BEDT-TTF)^0 [35]. Figure 3 is a projection of the cation-radical layer of α-(BEDT-TTF)$_2$TlHg(Se$_{0.875}$S$_{0.125}$CN)$_4$ along the b-axis. It is the typical cation-radical layer present in the so called α-phases. It is constructed from two nonequivalent stacks parallel to the c-axis. One of them is formed by the I and I$_i$ cation-radicals while the other contains the II and III ones. The stacks $\cdots$I$\cdots$I$_i\cdot\ \cdot$I$_c\cdot\ \cdot$ and $\cdot\ \cdot$III$\cdots$II$\cdot\ \cdot$III$_c\cdots$ pack side-by-side along the a-axis. The dihedral angles between I-II, I-III and II-III are 74.7, 80.2 and 5.9°, respectively, which are almost identical to those of α-(BEDT-TTF)$_2$TlHg(XCN)$_4$ with X = S and Se [3, 4]. There are no short intrastack S$\cdot\ \cdot$S contacts in the donor layers of α-(BEDT-TTF)$_2$TlHg(Se$_{0.875}$S$_{0\ 125}$CN)$_4$. In contrast, many short interstacks contacts exist (Tab. IV). The number of short S$\cdots$S contacts in the α-Tl(Se$_{0.875}$S$_{0\ 125}$) and α-Tl(Se) salts is smaller and the contacts are longer than in the α-Tl(S) salt. This is the result of the larger volume of the unit cell of the former two salts.

The structure of the anion layer is shown in Figure 4. Each XCN group of this layer forms a bridge between the Tl^+ and Hg^{2+} cations, thus leading to a polymeric network in the ac-plane. This network contains the Hg^{2+} ions tetrahedrally coordinated with four X atoms from the XCN groups. The Hg-X interatomic distances are in the range 2.624 – 2.651(2) Å. The corresponding distances for the α-Tl(Se) and the α-Tl(S) salts are in the range 2.640 – 2.651(1) [3] and 2.541 – 2.567(2) Å [4], respectively. The coordination of the Tl^+ ion is quite typical: four short bonds on one side of the ion, and four longer bonds on the other [36]. The Tl ion is placed at the top of a pyramid and is bonded to four N atoms from the XCN groups. The Tl-N interatomic distances are in the range 2.96 – 3.09(1) Å. The corresponding parameters for the selenocyanate and the thiocyanate analogs are in the range 2.99–3.01(1) and 2.935–3.019(8) Å, respectively. Four longer Tl-X bonds complement the Tl coordination up to eight (a tetragonal antiprism). Their lengths are 3.427 – 3.608(2), 3.456 – 3.616(1), and 3.395 – 3.593(2) Å for the α-Tl(Se$_{0.875}$S$_{0.125}$), α-Tl(Se), and α-Tl(S) salts, respectively.

The room temperature conductivities of the mixed α-(BEDT-TTF)$_2$TlHg(Se$_{1-x}$S$_x$CN)$_4$ salts are 2 Ohm^{-1}cm^{-1} for x = 0.125, 0.6 – 1.6 Ohm^{-1}cm^{-1} for x = 0.225 – 0.325 and 15 Ohm^{-1}cm^{-1} for x = 0.450. They are stable metals without the low-temperature phase transition characteristic of several of the α-(BEDT-TTF)$_2$MHg(XCN)$_4$ salts [5–7, 10].

In conclusion, the α-(BEDT-TTF)$_2$TlHg(Se$_{0\ 875}$S$_{0.125}$CN)$_4$ cation-radical salt is still another member of the α-(BEDT-TTF)$_2$MHg(XCN)$_4$ family of isostructural cation-radical salts. All of them are two-dimensional organic metals and the metallic state in these salts is stable down to

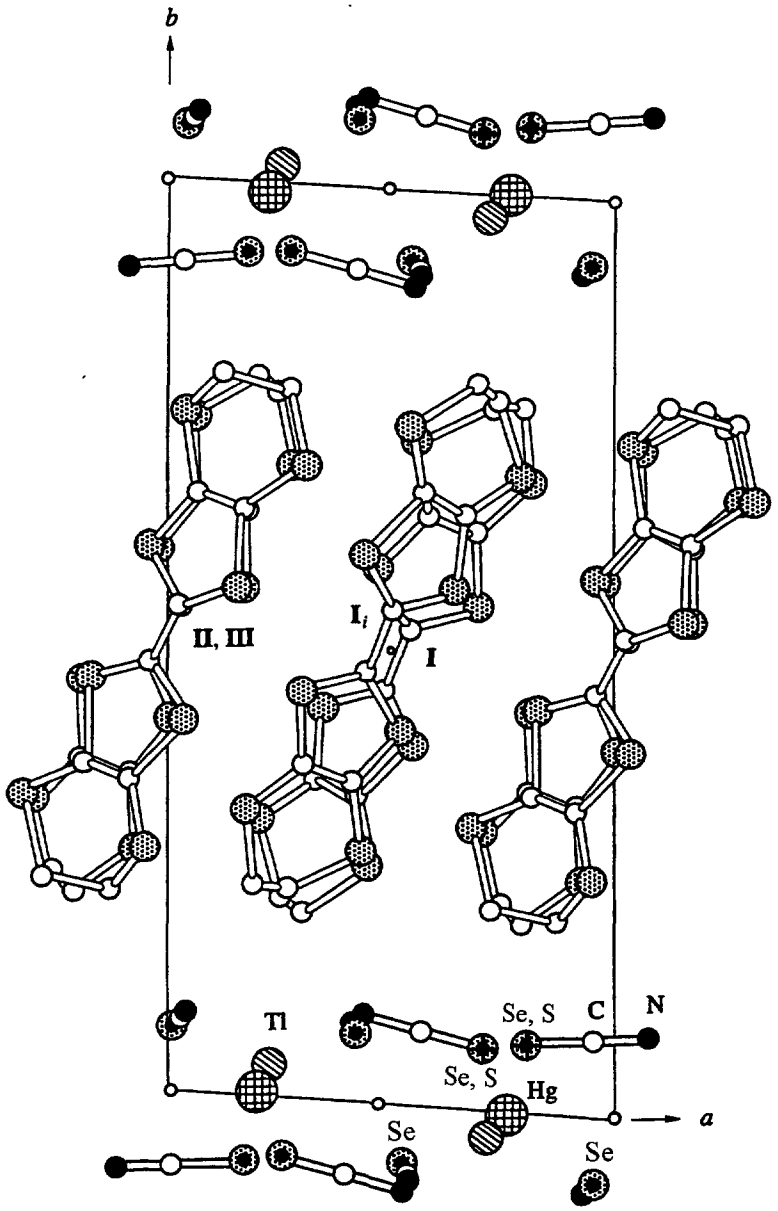

Fig. 1. — Structure of the α-(BEDT-TTF)$_2$TlHg(Se$_{0.875}$S$_{0.125}$CN)$_4$ salt projected along the *c*-direction. Symmetry operations for the BEDT-TTF cation-radicals are as follows: I, II, III: (x, y, z), I_i: $(1-x, 1-y, 1-z)$.

the lowest temperatures. In contrast, the cation-radical salts α-(BEDT-TTF)$_2$I$_3$ [23–25,28] and α-(BEDT-TTF)$_2$Cu(SCN)$_2$ [37,38] undergo a metal-to-insulator transition at 137 and 200 K, respectively, and the cation-radical salts α-(BEDT-TTF)$_2$IBr$_2$ [26] and α-(BEDT-TTF)$_4$PtBr$_6$ [27] are semiconductors [28,30]. In what follows we analyze in details the electronic structure of most of these salts.

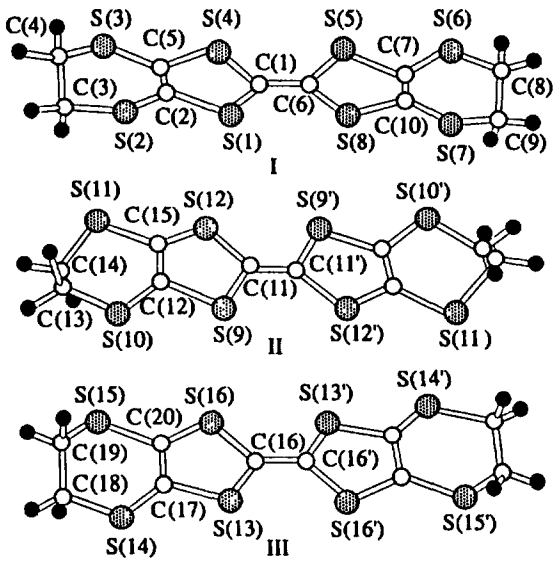

Fig. 2. — The (BEDT-TTF) cation-radicals I, II, and III.

4. Comparison of the Electronic Structures of α-(BEDT-TTF)$_2$MHg(XCN)$_4$ (M = NH$_4$, K, Tl; X = S, Se, Se$_{1-x}$S$_x$) and Related Phases

4.1. Band Structure and Fermi Surfaces. — The calculated band structure for the donor layer of α-(BEDT-TTF)$_2$TlHg(Se$_{0.875}$S$_{0.125}$CN)$_4$ is shown in Figure 5a. With the average oxidation state of (BEDT-TTF)$^{+1/2}$ there are six electrons to fill the HOMO bands. Since the third and fourth bands (from the bottom) overlap, the system should be metallic and the Fermi surface should exhibit both electron and hole contributions. The calculated Fermi surface is shown in Figure 6a. As usual in the α-(BEDT-TTF)$_2$MHg(XCN)$_4$ family [2, 14, 21, 22], the hole contribution is closed whereas the electron contribution is open and parallel to the c^* direction. Looking at the Fermi surface of Figure 6a it is obvious that the area of the closed part is smaller that 16%, *i. e.*, the approximate value reported for all other phases of this family. Is this difference something inherent to the new phase? In order to address this question we have carried out exactly the same type of calculations for α-(BEDT-TTF)$_2$KHg(SCN)$_4$ using the crystal structures determined at 298 K and 104 K. α-(BEDT-TTF)$_2$TlHg(XCN)$_4$ (X = S and Se) and α-(BEDT-TTF)$_2$NH$_4$Hg(SCN)$_4$. The calculated Fermi surfaces are reported in Figures 6b-f. It can be easily seen that the area of the closed part of the Fermi surface for all X(S) phases is clearly larger than those for the Tl(Se) and Tl(Se$_{0.875}$S$_{0.125}$) salts [39].

The calculated band structure for the Tl(S) salt is shown in Figure 5b. Although there are some differences in details, the band structures for all M(S) salts are very similar so that only that for Tl(S) is reported here. The band structure of the Tl(Se) salt is practically identical to that of Figure 5a and is not reported neither. The main difference between the two band structures of Figure 5 is that the third and fourth bands nearly touch along the X $\rightarrow$ M line for the Tl(S) salt whereas they are clearly separated in the case of Tl(Se$_{0.875}$S$_{0.125}$). This leads to a very narrow 1D part and consequently to a small area for the Tl(Se$_{0.875}$S$_{0.125}$) and Tl(Se) salts. Though, the general shape of the two overlapping bands is very similar.

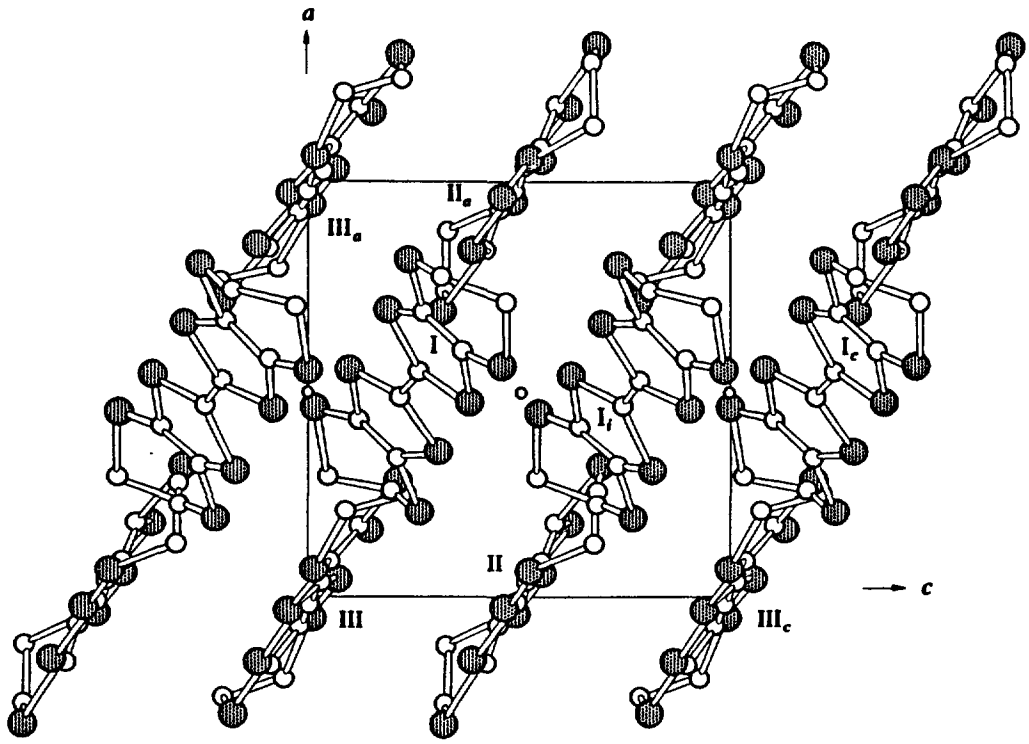

Fig. 3. — Structure of the cation-radical layer of α-(BEDT-TTF)$_2$TlHg(Se$_{0.875}$S$_{0.125}$CN)$_4$ projected along the *b*-direction. Symmetry operations for BEDT-TTF cation-radicals are as follows: I, II, III: (x, y, z), I$_i$: $(1-x, 1-y, 1-z)$, IIa and IIIa: $(1+x, y, z)$, Ic and IIIc: $(x, y, 1+z)$.

Before looking in detail at the nature of the band structures of Figure 5 let us come back to the Fermi surfaces of Figure 6. The difference in area between the Fermi surfaces of the Tl(Se)/Tl(Se$_{0.875}$S$_{0.125}$) and the M(S) salts is not the only interesting observation we can make. It can also be seen that the warping of the 1D part of the Fermi surfaces for Tl(S) and K(S) (both at 298 and 104 K) is very regular whereas those for the Tl(Se), Tl(Se$_{0.875}$S$_{0.125}$) and NH_4(S) are quite irregular. This observation can be connected to the fact that the first two salts exhibit the low temperature resistivity anomaly believed to originate in the nesting of the 1D part of the Fermi surface whereas the last three do not. Thus, one question we should address here is if there is some correlation between the warping of the open part of the Fermi surface and the crystal structure. Another observation which can be made is that the area of the closed part of the Fermi surface of the K(S) salt at 298 and 104 K almost does not change. Since the transfer integrals change with temperature, this result seems at first sight surprising. More specifically, it seems difficult to understand given the reported increase of the area of the Fermi surface under pressure [12, 21]. Although pressure and thermal contraction do not necessarily lead to the same modifications, at least some relation could be expected.

4.2. How the Different Donor·· Donor Interactions Influence the Electronic Structure. — The results of the previous section bring about many questions concerning the differences and similarities between the electronic structures of the salts, and more specifically,

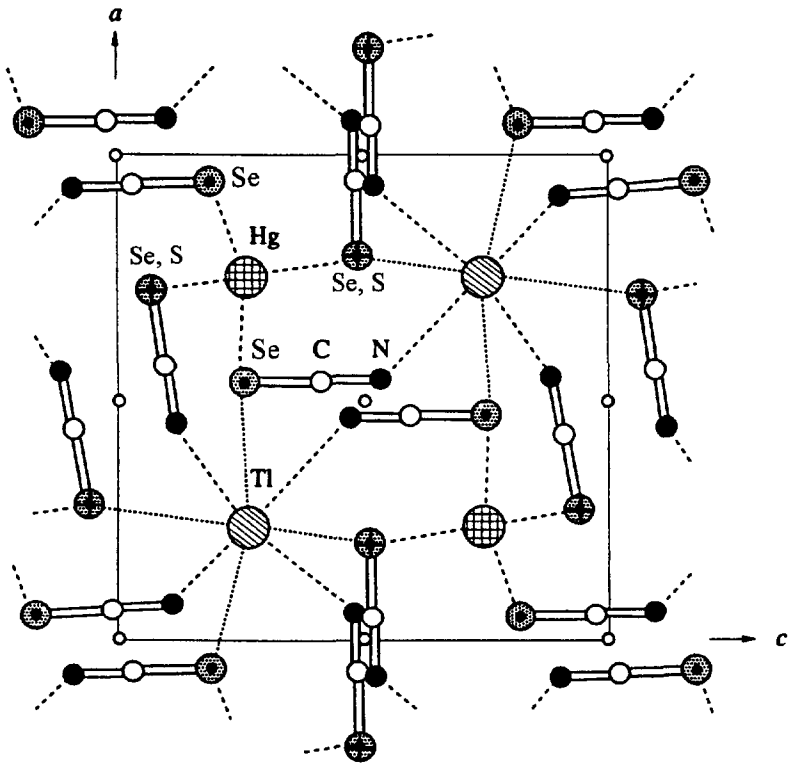

Fig. 4. — Anion arrangement of α-(BEDT-TTF)$_2$TlHg(Se$_{0.875}$S$_{0.125}$CN)$_4$ projected along the b-axis.

concerning the link between the calculated results and the crystal structure of the different salts. This is a difficult question to address because of several reasons. First, the experimental information about the Fermi surface comes from magnetoresistance experiments performed at low temperature. In contrast, the crystal structures on which the computations are based have been determined at considerably higher temperatures. Is the effect of the thermal contraction negligible as suggested by our results for the K(S) salt at 298 and 104 K? But if the answer was yes, why then do we calculate a considerably smaller area for the closed portion of the Fermi surface of the Tl(Se) salt for which we know that, at low temperatures, this area is practically the same as for all other M(S) salts [20]? Second, the structures under pressure are not known at all and thus it is difficult to understand the effect of pressure on the Fermi surface. Third, the overall similarity of the band structures and the large number of different donor···donor interactions (*i.e.*, transfer integrals) in the donor layer (seven) makes difficult to correlate the crystal and electronic structure. Under such circumstances the easiest way to tackle the problem is by using the well known tight-binding equations for the energy *vs.* **k** dependence as a function of the different transfer integrals of the lattice [34]. The effect of pressure and thermal contraction or the role of the different donor·· donor interactions, can then be modeled by systematically changing the different transfer integrals. Later, one can look at what structural changes can lead to these variations of the individual transfer integrals and discuss their likeliness.

Table IV. — *S···S short contacts ($r \leq 3.70$ Å) between the BEDT-TTF donors in the crystals of α-(BEDT-TTF)$_2$TlHg(XCN)$_4$, where X = S, Se and ($Se_{0.875}S_{0.125}$).*

Contact	Se	$Se_{0.875}S_{0.125}$	S	BEDT-TTF[a]
S1···S10	—	—	3.685(2)	I-II
S1···S14	3.495(3)	3.503(7)	3.483(3)	I-III
S2···S10	3.617(4)	3.628(7)	3.591(2)	I-II
S2···S14	3.503(3)	3.499(6)	3.455(2)	I-III
S3···S11	3.652(3)	3.662(7)	3.625(2)	$I\text{-}II_a$
S3···S15	3.529(3)	3.520(7)	3.473(2)	$I\text{-}III_a$
S3···S16	3.523(3)	3.515(6)	3.490(2)	$I\text{-}III_a$
S3···S12	3.684(3)	3.694(7)	3.674(2)	$I\text{-}II_a$
S5···S10′	3.558(4)	3.561(7)	3.544(3)	$I\text{-}II_a$
S5···S14′	3.681(3)	3.680(6)	3.653(2)	$I\text{-}III_a$
S6···S14′	3.658(3)	3.659(7)	3.611(2)	$I\text{-}III_a$
S7···S11′	3.676(3)	3.660(7)	3.637(2)	I-II
S7···S12′	3.559(3)	3.553(6)	3.539(2)	I-II
S7···S15′	—	—	3.665(2)	I-III
S7···S16′	3.680(3)	3.686(7)	3.659(3)	I-III

[a] For the symmetry operations of the BEDT-TTF donors see caption to Figure 3.

The transfer integrals used as a starting point for our model study have been calculated from the 104 K crystal structure [2] of the K(S) salt [41]. On the basis of the presently known crystal structures, these transfer integrals should provide the best approximation to the low temperature and ambient pressure Fermi surface. The different transfer integrals are defined in Figure 7, which is a representation of the slab where the donor molecules are viewed approximately along their long axis. Three of these transfer integrals (c_1 to c_3) will be referred to as intrachain transfer integrals and the remaining four (p_1 to p_4) as interchain transfer integrals [40]. As discussed in the previous section, the donor lattice contains two different types of donor chains (A and B). Chain A contains only one type of donors (I, I_1) whereas chain B contains two different types (II and III).

In our study, the transfer integrals were varied up to values of ±20% for each individual transfer integral as well as for specific groups of integrals. Inclusion of dissimilarity in the molecules by decreasing the energy of the $HOMO_{II}$ and $HOMO_{III}$ with respect to that of the $HOMO_I$ up to 0.2 eV was also carried out. The main results of this study are as follows:

a) The increase of both intrachain and interchain transfer integrals by the same amount leaves the area of the closed part of the Fermi surface unchanged.

b) An increase of all interchain transfer integrals (p-type) leads to an increase of the closed part of the Fermi surface. For instance, an increase of these integrals by 10% and 20% leads to an increase of 10.4% and 18.8% of the area, respectively. The transfer integrals p_1 and p_4 play the dominant role on this interaction.

c) An increase of all intrachain transfer integrals (c-type) leads to a decrease of the closed part of the Fermi surface. For instance, an increase of 10% and 20% of these transfer integrals leads to a decrease of 9.9% and 17.8% of the area, respectively. Such decreases are mostly imposed by the transfer integral c_2 alone.

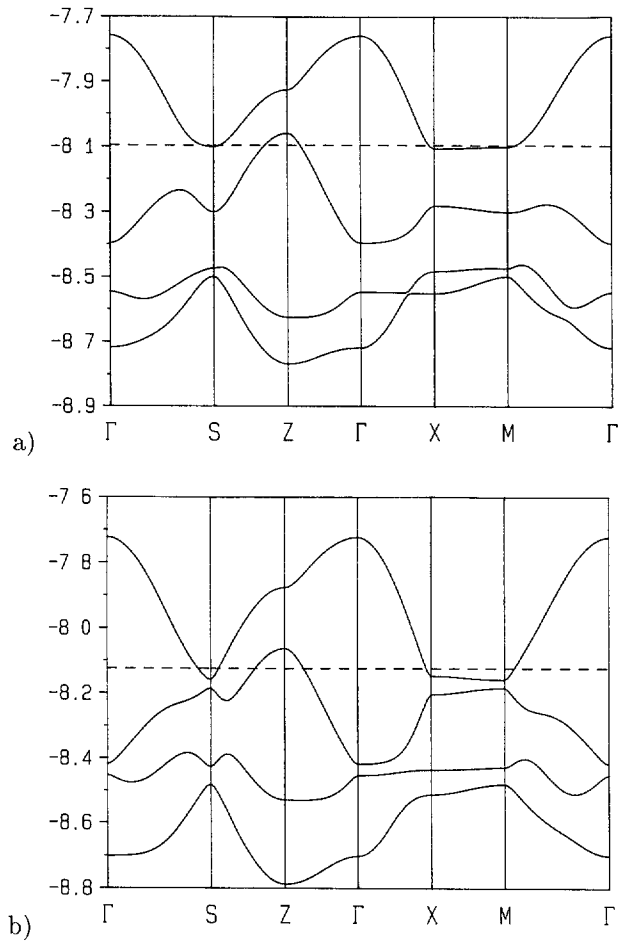

Fig. 5. — Calculated dispersion relations for the HOMO bands of (a) α-(BEDT-TTF)$_2$Tl Hg(Se$_{0\,875}$S$_{0\,125}$CN)$_4$ and (b) α-(BEDT-TTF)$_2$TlHg(SCN)$_4$, where the dashed lines indicate the Fermi level. Γ, X, Z. S, and M refer to the wave vectors (0, 0), ($a^*/2$, 0), (0, $c^*/2$), ($-a^*/2$, $c^*/2$) and ($a^*/2$, $c^*/2$), respectively. Energies are given in eV.

d) A decrease in the value of $HOMO_{II}$ and $HOMO_{III}$ with respect to that of $HOMO_I$ causes the area of the closed part of the Fermi surface to decrease. For instance, decreasing both $HOMO_{II}$ and $HOMO_{III}$ by 0.1 eV and 0.2 eV decreases the area of the closed part of the Fermi surface by 13.2% and 36.6%, respectively. However, since changes of 16.6% and 39.6% were obtained when only $HOMO_{II}$ was decreased by the same amount, the dominant role of $HOMO_{II}$ is clear.

With these results in mind it is easy to answer some of the above mentioned questions concerning the α-(BEDT-TTF)$_2$MHg(XCN)$_4$ phases. First, the almost nil effect of thermal contraction on the area of the closed part of the Fermi surface of the K(S) salt. Thermal contraction, as judged from the transfer integrals calculated from the 298 and 104 K crystal structures of this salt, leads to an increase of both interchain and intrachain transfer integrals. Consequently, the two contributions cancel each other leading to practically no change in the

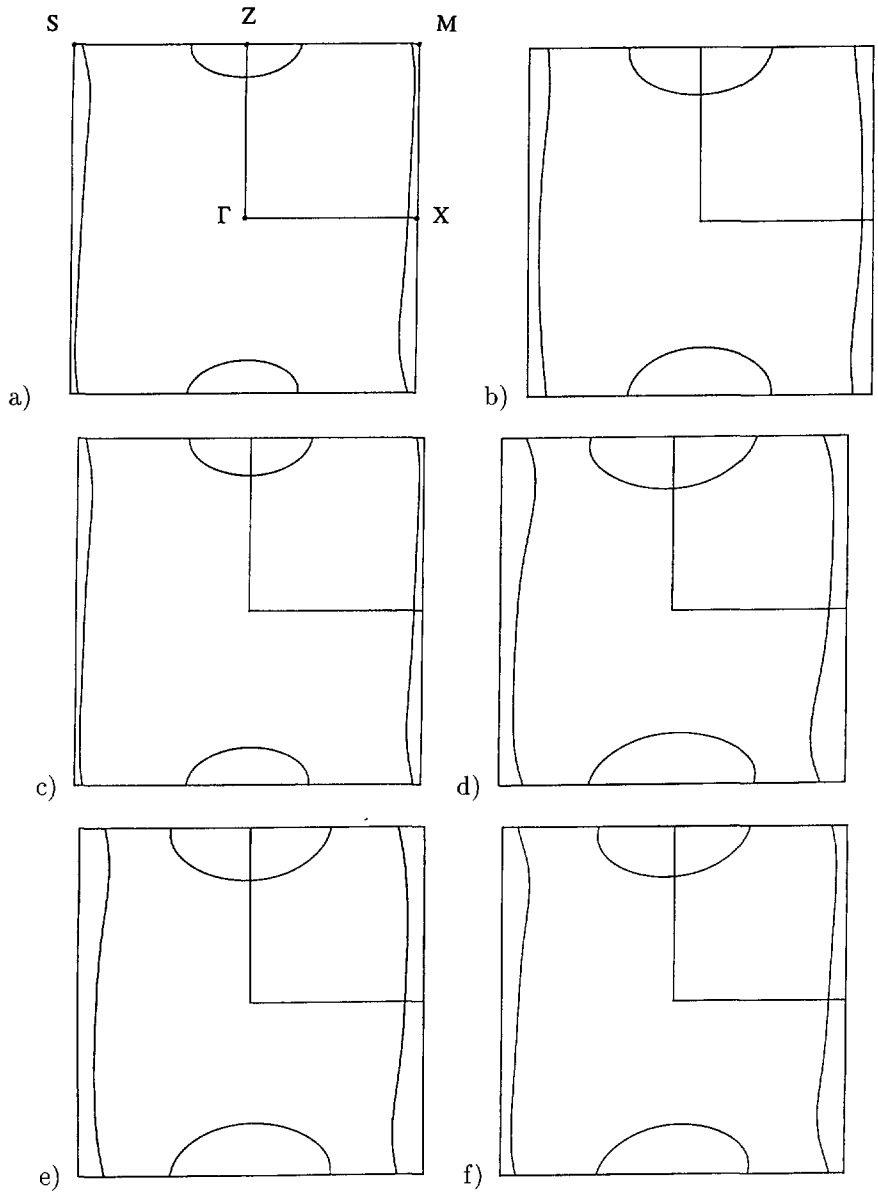

Fig. 6. — Calculated Fermi surfaces for: a) α-(BEDT-TTF)$_2$TlHg(Se$_{0.875}$S$_{0.125}$CN)$_4$, b) α-BEDT-TTF)$_2$TlHg(SCN)$_4$, c) α-(BEDT-TTF)$_2$TlHg(SeCN)$_4$, d) α-(BEDT-TTF)$_2$KHg(SCN)$_4$ (using the crystal structure determined at 298 K), e) α-(BEDT-TTF)$_2$KHg(SCN)$_4$ (using the crystal structure determined at 104 K) and f) α-(BEDT-TTF)$_2$NH$_4$Hg(SCN)$_4$. Γ, X, Z, S, and M refer to the wave vectors (0, 0), ($a^*/2$, 0), (0, $c^*/2$), ($-a^*/2$, $c^*/2$) and ($a^*/2$, $c^*/2$), respectively.

calculated areas. Second, these results also suggest how area increases like those reported under pressure [12, 21] can be obtained. For example, the closed portion of the Fermi surface of the Tl(Se) salt was found to increase by 21% under 11 kbar [21]. As both the a and c crystallographic parameters decrease under pressure, one may expect that both interchain and

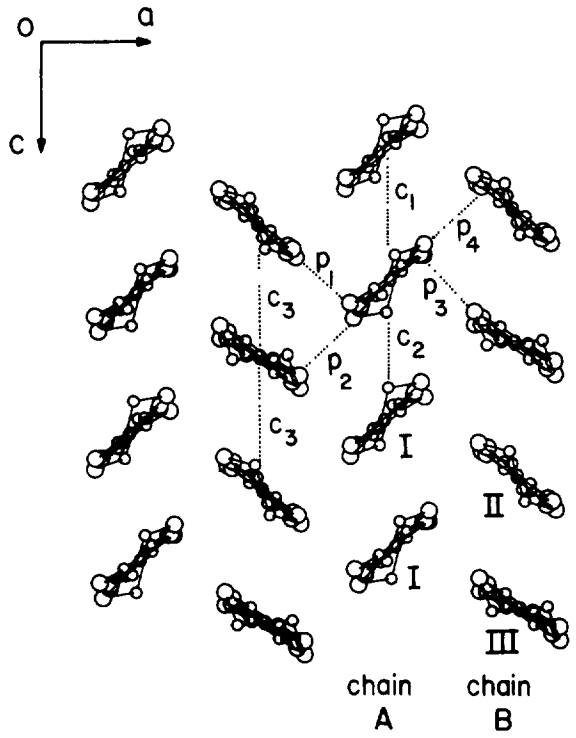

Fig. 7. — Perspective view of a BEDT-TTF layer of α-(BEDT-TTF)$_2$MHg(XCN)$_4$ where the different interactions are defined [40]. Each molecule is viewed approximately along its central C = C bond and the hydrogen atoms are not shown for simplicity.

intrachain transfer integrals should increase (as for thermal contraction). An increase in c_2 of about 20% leads to a decrease in the area of the closed part of about 20% whereas the other intrachain transfer integrals have an almost nil effect. This is compared to the above mentioned increase of 18.8% of the area for increases of 20% in the interchain transfer integrals. Thus the observed change in the surface area may be obtained by a motion which increases the p-type interactions (especially those of p_1 and p_4) but leaves c_2 unchanged. In fact, it is quite easy to see what this motion is and that it is likely that it occurs under pressure. Calculations for the two donor molecules (I and I_i) involved in interaction c_2 show that:

a) If the interplanar distance between the two donors decreases, c_2 increases. For instance, a decrease of the interplanar distance by 0.05 Å leads to an increase of c_2 by about 7%.

b) If there is a sliding of one donor towards the other along the short axis of the molecules, c_2 decreases. A sliding of about 0.08 Å leads to a decrease in c_2 of about 7%. In fact, the large difference between the two transfer integrals along chain A ($c_1 = -0.012$ eV and $c_2 = 0.140$ eV in the 104 K structure of α-(BEDT-TTF)$_2$KHg(SCN)$_4$) is largely due to this type of sliding. The interplanar distances between the two donors differs only by 0.05 Å for the two interactions. However, as can be easily seen just by visual inspection of Figure 7, the sliding along the short axis of the molecules is quite different. In fact, this sliding is around 0.7 Å larger in c_1 than in c_2 [2,14] and is the major geometrical parameter responsible for the difference in the magnitude of these two integrals.

Thus, even if pressure leads to an increase in c_2 by decreasing the interplanar distance, such change can be easily canceled by a small sliding motion along the short axis of the molecule. Furthermore, a 20% increase in the p-type integrals is an entirely plausible fact. Consider that, as mentioned above, the major change in the area of the closed portion of the Fermi surface is related to p_1 and p_4. Just thermal contraction from 298 K to 104 K for the K(S) salt leads to increases of these two integrals by 12% and 8%, respectively. Thus, it seems likely that the change in Fermi surface area that occurs in these salts under pressure is due to the increase of the p-type interactions relative to the c-type ones *via* a sliding of the donors associated with interaction c_2 as well as an overall compression of the lattice.

We may now turn to the question of why the calculated area of the closed portion of the Fermi surface for the Tl(Se) and Tl($Se_{0.875}S_{0.125}$) salts is smaller than those for all M(S) salts whereas, according to the magnetoresistance experiments, it should be almost identical. We discard that computational problems or inadequacies in the crystal structure determination are at the origin for this fact because of the following reasons. First, the calculations have been carried out using exactly the same exponents and parameters for all salts. Since only the donor layers are considered in the calculation, if there was some methodological problem, it should appear in all computations and not only in those for the Tl(Se) and Tl($Se_{0\ 875}S_{0.125}$) salts. Second, the two structures have good R factors and no problems were found during the refinement. The heart of the problem lies in the fact that the crystal structures on which the calculations are based are those at room temperature, whereas the magnetoresistance experiments are carried out at very low temperature. The discussion of the previous paragraphs suggests two possible explanations for this question, both of which are based on the fact that the apparent problem is exhibited by the salts having Se either as the majoritary or as the only chalcogen in the anion layer. Since the movements of the donor molecules are influenced through hydrogen bonding interactions (X$\cdots$ H-C) by the nature of the chalcogen in the polymeric anion network, it is possible that the modifications brought about by the thermal contraction are slightly different for the Se-containing salts. A likely possibility is that the sliding motions inside the lattice of the Se-containing salts as temperature decreases have an effect on increasing the interactions between chains A and B (and more specially interactions p_1 and p_4) but not those within the chains. This means that the effect of thermal contraction for the Se-containing salts would be similar to the pressure effect on the S-containing salts. The area would thus continuously increase when temperature goes down and eventually reach the same value as the S-containing salts at low temperature. A second, probably more likely explanation, is based on the fact that whereas the strength of the different donor$\cdots$donor interactions are quite similar for the S- and Se-containing salts, the BEDT-TTF donors exhibit different central C = C bond lengths only in the Se-containing salts. According to our calculations, the shorter bond lengths for donors II and III leads, as intuitively expected, to HOMO energies considerably lower ($\sim$ 0.2 eV) than those for donor I. As noted above, our model study shows that lowering the $HOMO_{II}$ energy has a large effect in decreasing the area of the closed part of the Fermi surface. Thus, it is likely that the area of the room temperature Fermi surface is quite small because of this short C = C bond length and that as temperature goes down the dissimilarity between the three donor molecules decreases and the C = C bond lengths become quite uniform at low temperature. Given the similarity in donor$\cdots$ donor interactions this would lead, at the temperature of the magnetoresistance experiments, to practically the same area as the S-containing salts. It is clear that low temperature structural work is absolutely needed in order to elucidate which of the two possibilities is the correct one.

At this point we should consider the recently reported results concerning the new K(Se) salt. The three different donor molecules in this Se-containing salt exhibit two very different central C = C bond lengths (see Tab. V). We do not report detailed calculations on this salt

Table V. — *Central C=C bond lengths (Å) of BEDT-TTF I, II and III in α-(BEDT-TTF)$_2$MHg(XCN)$_4$ (M = Tl, X = S, Se, Se$_{0.875}$S$_{0.125}$ and M = K, X = S, Se).*

BEDT-TTF	Tl(S)	Tl(Se)	Tl(Se$_{0.875}$S$_{0.125}$)	K(S)	K(Se)
I	1.37(1)	1.39(1)	1.42(2)	1.36(2)	1.35(3)
II	1.37(1)	1.33(1)	1.34(2)	1.37(2)	1.27(3)
III	1.36(1)	1.33(1)	1.33(2)	1.37(2)	1.28(3)
	[4]	[3]	this work	[2]	[22]

because the unreasonably short values for the C = C bond lengths of donors II and III would strongly influence the shape of the Fermi surface. However, what is clear on the basis of our model results and the crystal structure information about the K(S) and K(Se) salts is that the Fermi surfaces of the two salts can not be practically identical, as calculated by Sasaki *et al.* [22]. The area of the room temperature Fermi surface of the K(Se) salt should be smaller. How this affects the actual Fermi surface and in particular the warping of the 1D portion is something which must await a better room temperature as well as low temperature crystal structures. However, what can plausibly be said even at the present moment is that its Fermi surface is likely to have a stronger resemblance to those of the Tl(Se) and Tl(Se$_{0.875}$S$_{0.125}$) salts than to those of the K(S) or Tl(S) salts. That the three presently known Se-containing salts all have donor molecules in apparently different oxidation states and also a similar physical behavior which differs from those of the S-containing salts, is something that in view of the present study is not so surprising, even if not yet well understood. It is also a reminder of how careful one needs to be when using model tight binding calculations to evaluate the Fermi surface. The similarity in the Fermi surfaces reported for the K(S) and K(Se) salts presumably comes from the fact that the influence of the different HOMO energies (and thus, of significant details of the crystal structure) on the electronic structure was not taken into account in the calculations [42].

4.3. Dimensionality and Fermi Surface of the α-(BEDT-TTF)$_2$MHg(XCN)$_4$ Salts. — Now that the topology of the Fermi surface has been explored in terms of the different intermolecular interactions and that the effects of temperature and pressure have been discussed, a simple conceptual model can be constructed for these systems. Some of the questions to which we would like to answer are the following. What is the meaning of dimensionality in these systems? Why do the Fermi surfaces of these salts possess both one and two dimensional portions? Is there actually a structural motif causing this, *i.e.*, is there actually a 1D chain here? If so, then why is there a closed 2D orbit on the Fermi surface as well? The above transfer integral study also raises the question of why are the integrals p_1 and p_4 more important in determining the surface area of the closed portion than the other p-type integrals. For this matter why does c_2 play such a dominant role in this system as well? Finally, why does the HOMO$_{II}$ energy have such an important effect on the Fermi surface area and not those of HOMO$_I$ and HOMO$_{III}$? A glance at the structure in Figure 7 reveals that apparently there should be no reason for this behavior.

For this end, consider the transfer integrals of Table VI. Of the c-type interaction energies only c_2 is sizable in chain A. Although from just a visual inspection this chain appears to be just that, a chain, in terms of the electronic structure it is a series of weakly interacting dimers. From now on we will call them c_2 dimers. Consider now Figure 7 in the light of this fact. It can be seen that the integrals p_2 and p_3 are different from their counterparts p_1 and p_4 in their

orientation with respect to this dimer. In fact, we can see that the different c_2 dimers interact through donors III (interactions p_2 and p_3) to form a chain along the a direction. Thus, at least conceptually, it is tempting to consider the lattice of the α-(BEDT-TTF)$_2$MHg(XCN)$_4$ phases as being made of chains of donors III and I (c_2 dimers) which communicate through donors II.

To further explore this idea, we carried out a series of model calculations where, taking the transfer integrals calculated for the 104 K structure of the K(S) salt as the starting point, we gradually decreased the values of the p_1, p_4 and c_3 transfer integrals while keeping the other integrals constant. In such a way we gradually isolated the suggested chains within the lattice. The band structure of the lattice was calculated as a function of the parameter γ, which defines the different values of the p_1, p_4 and c_3 transfer integrals (t') through the relationship $t' = \gamma t$, where t refers to the value in the 104 K crystal structure. The results are shown in Figure 8. For $\gamma = 1$ the band structure is very similar to the results of the full calculations (see Fig. 5a for instance). For $\gamma = 0$ the band structure consists of a flat band, that of the noninteracting $HOMO_{II}$ levels, and a set of three bands characteristic of the chain along a. It is important to understand the topology of these three bands. Looking carefully at them it is easily seen that in fact they result from the interaction of a flat band (the second band at Γ) and two dispersive ones. When analyzing the orbital character of these bands it can be seen that the major components of the lower/upper dispersive bands are the bonding/antibonding combinations of the HOMOs of the c_2 dimer. The bonding/antibonding levels of the different c_2 dimers interact through the $HOMO_{III}$ and thus acquire dispersion (of course, leading to bands with opposite slope) along the $\Gamma \rightarrow X$ direction. Since the $HOMO_{III}$ levels are energetically in between the bonding and antibonding HOMO levels of the c_2 dimer, they interact in a stabilizing way with the antibonding level but in a destabilizing way with the bonding one leading to a quite flat band.

Thus, the nature of the upper dispersive band and the completely flat one of Figure 8a ($\gamma = 0$) are easy to understand. It is these two bands which are going to lead to the two partially filled bands of the α-(BEDT-TTF)$_2$MHg(XCN)$_4$ phases. This can be clearly seen in Figure 8. When we gradually switch the p_1, p_4 and c_3 interactions (*i.e.*, γ changes from 0 to 1) the bands of the two subsystems mix. The originally flat band being in the middle of the diagram, mixes with all other bands and looses any trace of its original shape, leading to a band dispersive in any direction. The originally upper dispersive band is pushed up in energy but being the upper one, interacts essentially with the originally flat band and changes much less its shape. The important point however is that the shape is practically unaltered at the bottom of the band. Thus, there is a strong memory of the chain of c_2 dimers and donors III in the bottom of the upper band of the α-(BEDT-TTF)$_2$MHg(XCN)$_4$ phases. Thus, even though there is a 2D slab of donors in this system, the electrons at the bottom of the upper band experience significant 1D interactions and consequently contribute with 1D electron pockets to the Fermi surface.

As mentioned, the third band originates from the $HOMO_{II}$ levels and its strong dispersion along all directions is caused by the switching of the p_1, p_4 and c_3 interactions. Hence, this band can be described as arising from the cross linking of the chains of the c_2 dimers and donors III through donors II. Therefore the following physical model can be suggested to describe the electronic structure of the α-(BEDT-TTF)$_2$MHg(XCN)$_4$ phases. The electron pockets of the Fermi surface arise from the chains of c_2 dimers and donors III along the a direction. The hole pockets of the Fermi surface originate from the coupling of such chains through donors II. Thus, the carriers of the Fermi surface of these phases *see* different aspects of the lattice. This model is schematically presented in Figure 9. With reference to this figure, the electron carriers only feel the interactions among the chains of donors in black whereas the hole carriers

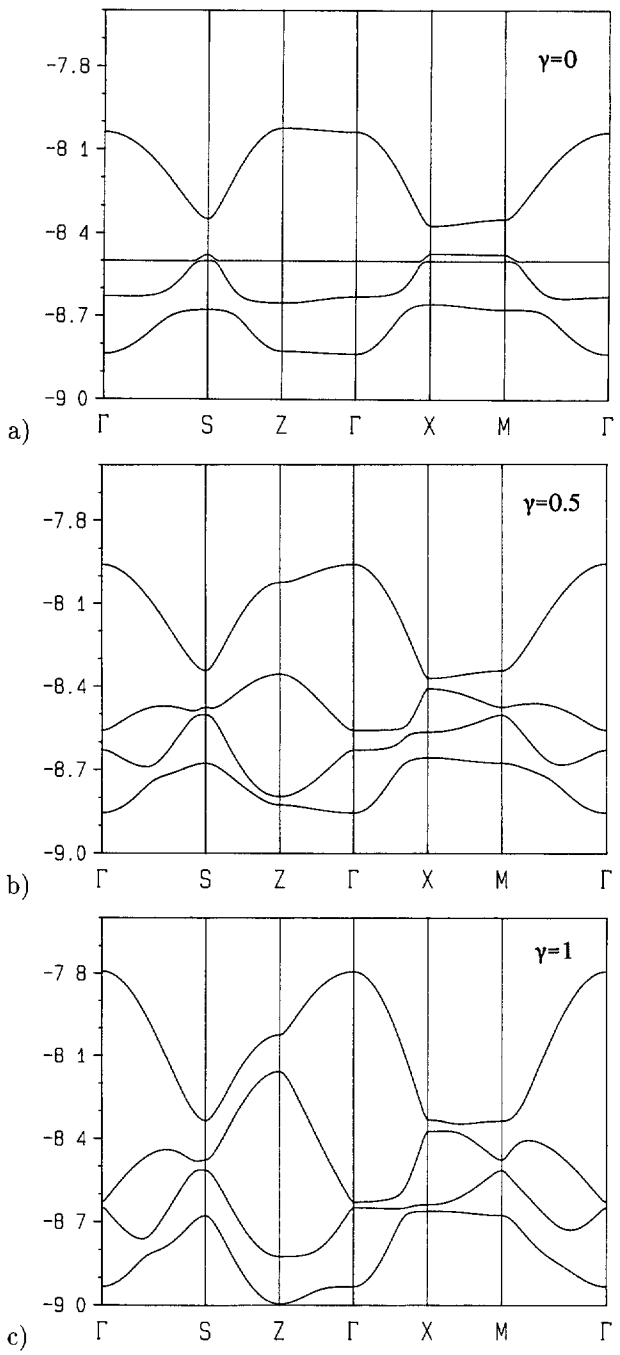

Fig. 8. — Model band structure for the α-(BEDT-TTF)$_2$MHg(XCN)$_4$ phases as a function of the parameter γ. The tight binding band structures were calculated on the basis of the transfer integrals evaluated for the 104 K structure of the K(S) salt. The γ parameter defines the different actual values of the p_1, p_4 and c_3 transfer integrals (t') used in the model calculations through the relationship $t' = \gamma t$, where t refers to the value in the 104 K crystal structure. All other transfer integrals were kept at their t values. Energies are given in eV.

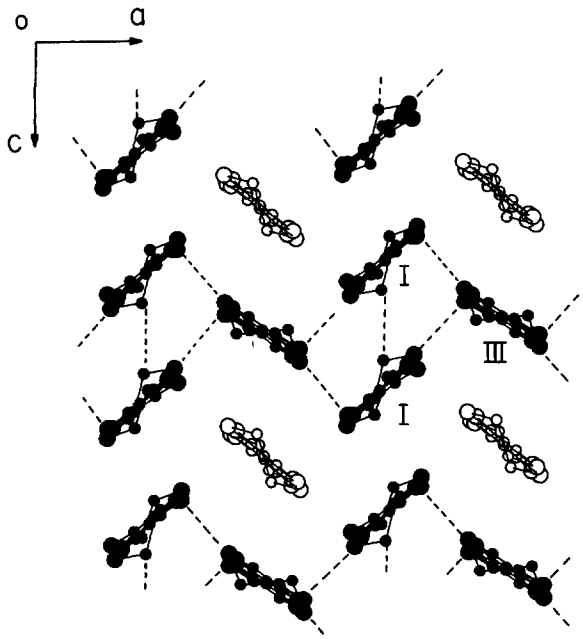

Fig. 9. — Schematic representation of the donor lattice of the α-(BEDT-TTF)$_2$MHg(XCN)$_4$ salts illustrating the nature of the "chains" leading to the 1D portion of the Fermi surface. The donors of the "chains" are shown with filled atoms and the "intrachain" interactions are marked with dotted lines.

feel all the interactions. At first sight this conclusion can appear as quite strange. However it is not. The reason lies again in the topology of the lattice. Because of the geometrical nature of the p_1 and p_4 interactions, *i.e.*, those which are largely responsible for the coupling of the chains, their contributions can add or can compensate depending on the phase of the different HOMOs. Whereas in the second case the 1D character survives, in the first one it completely disappears. The bottom of the fourth band lies in a region of the Brillouin zone where such phases impose a near cancellation of the p_1 and p_4 interactions whereas the opposite is true for the top of the third band. This is why we can say that the electrons and holes of these phases see different aspects of the donor lattice.

As a matter of fact this model, simple as it may be, makes it very easy to understand most of the results of our theoretical study and thus it is probably a useful conceptual framework by which new experimental results can be rationalized. For instance, the 2D surface area was found to strongly depend on the p_1 and p_4 interactions. This is because when the cross links between the chains increase, the system that the holes feel is more 2D and thus, the closed Fermi surface orbit becomes larger. The c_2 interaction was found to have the opposite effect. It is clear from our discussion that the c_2 transfer integral controls the separation between the upper/lower bands of the chain, *i.e.*, of the bands arising from the antibonding/bonding levels of the dimer. When c_2 increases, the separation between the bonding/antibonding levels of the dimer increases leading as a whole to a higher energy for the fourth band and thus, to a lower semimetallic overlap with the third band. This model explains also the dependence of the Fermi surface area on the $HOMO_{II}$ energy. As the $HOMO_{II}$ level is lower, the initial nondispersive band (from which the third band originates) will also lie lower in energy and thus, the smaller will be the semimetallic overlap and the Fermi surface area. When comparing different salts

this is true provided that the strength of the donor···donor interactions is not very different. As we have shown above, this is indeed the case for the different α-(BEDT-TTF)$_2$MHg(XCN)$_4$ salts.

It is not difficult to see how these ideas can be used to understand some experimental observations concerning these phases. For instance, it is clear from our proposed model (and we have verified this with model calculations) that the asymmetry of the 2D orbit with respect to the Z $\rightarrow$ M line of the Brillouin zone strongly depends on the relative value of the p_1 and p_4 interactions. As can be seen in Figures 7 and 9, the p_4 interaction acts in the $a-c$ direction whereas the p_1 interaction acts in the $a+c$ direction. If these two integrals are of different magnitude there is different coupling between the chains in these two directions. This asymmetric coupling of the 1D chains can thus lead to such an asymmetry of the 2D hole Fermi surface if under the conditions of the measurement the difference between the p_1 and p_4 interactions is strong enough. For instance, such asymmetry has been reported for the K(S) salt [43]. Thus, as also pointed out in our discussion of the effect of pressure on the Fermi surface area, the magnetoresistance experiments can indirectly provide important information on how pressure or thermal contraction affect different interactions of the donor layers.

Another aspect we would like to discuss is that of the warping of the 1D portion of the Fermi surface. As discussed before, this 1D portion results because of the approximate cancellation of the cross coupling interactions p_1, p_4, c_3 and, to a smaller degree, c_1. The major effect of the c_3 and c_1 interactions is to provide some cosine-like warping of the Fermi surface. However, the p_1 and p_4 interactions can perturb this simple scenario and, depending on their relative values, can make this warping more irregular. Both model calculations and an approximate analytical treatment show that the dispersion of the fourth band along a direction parallel to the X $\rightarrow$ M direction and not far from the border of the Brillouin zone is roughly governed by the relationship $|\Delta E| \approx |p_4 - p_1 - c_3 - c_1|$. From the transfer integrals calculated for all the salts studied we found that this value is very small. This is a direct reflection of the above mentioned cancellation of interactions which leads to the strong memory of the 1D interactions along the a direction for the electron carriers. This means that the 1D portion of the Fermi surface is highly sensitive to small changes in the crystal structure which can slightly modify the relative values of these transfer integrals. In other words, the nesting condition required to form the density wave state leading to the low temperature resistivity anomaly can be easily created or destroyed by the small geometric movements brought about by thermal contraction and pressure and this leads, at least partially, to the rich low temperature physics of these salts. Under such conditions, it is clear that the correlation pointed out at the beginning of this section, *i.e.*, that the warping is more irregular in the salts which do not show the resistivity anomaly, should not be overemphasized. The changes induced by the thermal contraction can completely invalidate the conclusions regarding this point made on the basis of the room temperature Fermi surfaces [14]. We need to wait for precise low temperature crystal structures in order to see if this correlation is kept down to these temperatures. Only then we will be able to go a step further in the analysis of the correlation between the crystal structure and the physical behavior.

4.4. Electronic Structure of the α-(BEDT-TTF)$_2$I$_3$, α-(BEDT-TTF)$_2$IBr$_2$ and α-(BEDT-TTF)$_4$PtBr$_6$ Salts. — To further investigate the factors involved in the electronic structure/physical properties relationships for the α phases of BEDT-TTF let us now consider the case of α-(BEDT-TTF)$_2$I$_3$. This salt was really the first α phase to be prepared [23–25]. α-(BEDT-TTF)$_2$I$_3$ is a room temperature metal and undergoes a metal to insulator transition at 135 K, the nature of which is not yet fully understood. The recent work by Dressel *et al.* [28] suggests that there is a band gap opening at the transition and that this happens

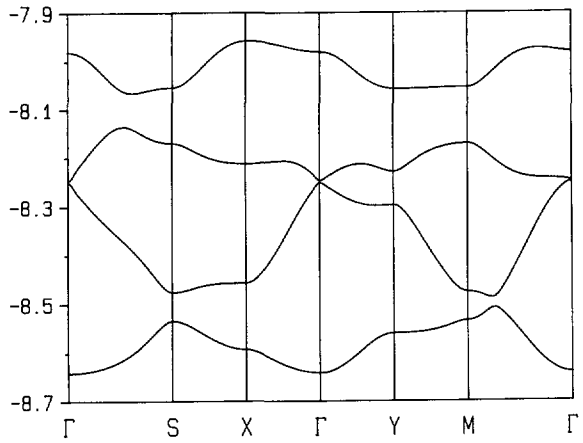

Fig. 10. — Calculated dispersion relations for the HOMO bands of the 298 K crystal structure [25] of α-(BEDT-TTF)$_2$I$_3$. Γ, X, Y, S, and M refer to the wave vectors (0, 0), ($a^*/2$, 0), (0, $b^*/2$), ($-a^*/2$, $b^*/2$) and ($a^*/2$, $b^*/2$), respectively. Energies are given in eV.

without any increase in the size of the unit cell. Although it was suggested that the metal to insulator transition could be associated with electron localization in different BEDT-TTF donors (as in α-(BEDT-TTF)$_2$MHg(XCN)$_4$ there are three different types of BEDT-TTF in the unit cell) [44], this possibility can now be discarded since the four donor molecules in the unit cell have been shown to be very similar both before and after the metal to insulator transition [25].

The calculated extended Hückel band structure using the 298 K crystal structure reported by Emge *et al.* [25] is shown in Figure 10. Before comparing this band structure with those of the α-(BEDT-TTF)$_2$MHg(XCN)$_4$ phases it should be noted that the crystallographic axes are different. Here the donor slabs lie in the (*ab*) plane and the *a*-axis runs along the direction parallel to chains A and B. In order to facilitate the comparison, the dispersion relations of Figure 10 have been plotted as for the band structures of the previous sections. The band structure below the transition is very similar and is not reported here. Both consist of four bands with the third and fourth bands being separated by a band gap. However these two bands become very close inside the Brillouin zone in a region not far from the Γ → S direction. The calculated band gap between these two bands is 0.03 eV for the 298 K structure and becomes 0.07 eV for the 135 K structure. With such a small band gap at 298 K, which in fact is not far from the thermal energy at this temperature, and the uncertainty in the Slater exponents used for the calculations which with just very minor changes can lead to the suppression of this band gap, we conclude that the metallic character of α-(BEDT-TTF)$_2$I$_3$ originates from the weak overlap of the third and fourth bands inside the Brillouin zone. However, in contrast with the situation in the α-(BEDT-TTF)$_2$MHg(XCN)$_4$ salts, our calculations suggest that both the electron and hole pockets should be closed. What also emerges from our calculations is that at low temperature the semimetallic overlap should decrease and eventually disappear. Before considering what motion is more likely to lie behind the 135 K transition let us first compare in detail the band structures of the α-(BEDT-TTF)$_2$I$_3$ and α-(BEDT-TTF)$_2$MHg(XCN)$_4$ salts.

The striking fact about the results of Figures 5 and 10 is that despite the similarity in the global topology of the donor layers, the band structures are quite different. A look at the transfer integrals of Table VI is however quite revealing. There are two important differences

Table VI. — *Transfer integrals (eV) for the different donor···donor interactions in some representative α-phases: α-(BEDT-TTF)$_2$TlHg(Se$_{0.875}$S$_{0.125}$CN)$_4$, α-(BEDT-TTF)$_2$TlHg(SCN)$_4$, α-(BEDT-TTF)$_2$I$_3$ (298 K) and α-(BEDT-TTF)$_4$PtBr$_6$.*

Interaction type	α-(BEDT-TTF)$_2$MHg(XCN)$_4$ [a] Tl(Se$_{0.875}$S$_{0.125}$)	Tl(S)	α-(BEDT-TTF)$_2$I$_3$ [a] (298 K)	α-(BEDT-TTF)$_4$PtBr$_6$ [b]
c_1	0.023	0.014	−0.043	0.028
c_2	0.139	0.128	0.072	−0.015
c_3	0 055	0.091	−0.033	−0.006
c_4	—	—	—	0 019
p_1	0.124	0.112	0 067	0 098
p_2	0.161	0 117	0 071	0 073
p_3	0.187	0 157	0.160	0.143
p_4	0 162	0.149	0.139	0.070

[a] For labeling of the interactions see Figure 7.

[b] For labeling of the interactions see Figure 11a.

between the two types of salts. First, c_2 is now considerably smaller so that the transfer integrals for chain A are no longer consistent with what one would expect for a chain of weakly interacting *dimers*. From the values of Table VI, this chain should now be best described as a series of weakly interacting *monomers*. This is a very important difference with the α-(BEDT-TTF)$_2$MHg(XCN)$_4$ salts. Geometrically, interaction c_2 is essentially identical in α-(BEDT-TTF)$_2$MHg(XCN)$_4$ and α-(BEDT-TTF)$_2$I$_3$. The main difference is the interplanar distance which is larger for α-(BEDT-TTF)$_2$I$_3$ and leads to the weaker interaction. Interaction c_1 is quite different in nature. In α-(BEDT-TTF)$_2$I$_3$ the two molecules have slid toward each other along the short axis of the molecule and the interplanar distance has changed. The result is a slight increase of this interaction which now approaches the decreased value of the c_2 one. The second difference is that interactions p_1 and p_2 are smaller in α-(BEDT-TTF)$_2$I$_3$.

To summarize, the change of the polymeric anionic layer for the chains of discrete I_3^- groups, although keeping the same type of organization for the donor slabs, it leads to weak and more uniform HOMO-HOMO interactions along the direction of chains I and II and also to weaker HOMO-HOMO interactions coupling these chains. From the electronic viewpoint, the donor layer of α-(BEDT-TTF)$_2$I$_3$ can be described as a 2D lattice of donor monomers interacting more weakly than in α-(BEDT-TTF)$_2$MHg(XCN)$_4$. This description is quite different from that put forward for the α-(BEDT-TTF)$_2$MHg(XCN)$_4$ salts. At this point we would like to emphasize that even if the weaker p-type interactions are important in leading to a smaller semimetallic overlap, the real difference between the topology of the band structures for the α-(BEDT-TTF)$_2$MHg(XCN)$_4$ and α-(BEDT-TTF)$_2$I$_3$ salts lies in the weaker c_2 interaction. The decrease on this interaction is such that the system has lost any memory of the bonding/antibonding levels of the c_2 dimers and hence of the · ·(I-I$_1$)· III· ·(I-I$_1$)· III··· chains in the donor lattice. The different I-I$_i$ interplanar spacing brought about by the use of different anions has thus a fundamental role in determining the electronic structure and consequently the physical properties of the BEDT-TTF α phases.

What can be said about the origin of the metal to insulator transition in α-(BEDT-TTF)$_2$I$_3$? Calculations using the crystal structures at 298 K and 120 K show that the c-type transfer integrals change significantly whereas most of the p-type integrals (except p_1) do not appreciably change [45]. In comparison with the changes induced by thermal contraction from 298 K to

104 K for the K(S) salt the changes are quite large. Thus, it may be safely concluded that there is more than just thermal contraction behind these changes. Model tight-binding simulations like those described for the α-(BEDT-TTF)$_2$MHg(XCN)$_4$ salts led to the conclusion that the magnitude of the band gap between the third and fourth bands is largely dominated by the c_1 and c_2 transfer integrals. Both an increase in absolute value of c_2 and a decrease in that of c_1 lead to an increase of the band gap [46]. Changes in c_3 and the p-type integrals seem to have a much smaller effect. Altogether, the two series of calculations suggest that the larger band gap we find for the 120 K structure is associated with the slight "dimerization" occurring in chain A. Consequently, we believe that this is the origin of the metal to insulator transition in α-(BEDT-TTF)$_2$I$_3$.

Two structural studies below the transition temperature of α-(BEDT-TTF)$_2$I$_3$ have been reported. These studies led to different conclusions as to what is the nature of the structural transition. Endres *et al.* [47] proposed that the major structural change seems to involve chains A which become more "dimerized". In contrast, Kagoshima *et al.* [48] proposed that the major structural changes affect chain B. Our study suggest that the proposal by Endres *et al.* is more appropriate. It is also worth pointing out that according to the low temperature crystal structures by Emge *et al.* [25] and Endres *et al.* [47], the main difference in the anion lattice (*i.e.*, the parallel chains of interacting I_3^- anions) between the 298 K and the low temperature structures is a motion involving the I_3^- units of one of the two chains. These I_3^- units interact through I$\cdots$H contacts mostly with the BEDT-TTF donors of chain A. We believe that all these results can be integrated into a simple scenario. Thus, at around 130 K a slight motion of one of the two I_3^- anions of the lattice induces a weak "dimerization" in the donors of chain A which leads to the opening of a band gap between the third and fourth HOMO bands of the lattice and thus to the metal to insulator transition.

That the α-(BEDT-TTF)$_2$I$_3$ and α-(BEDT-TTF)$_2$MHg(XCN)$_4$ salts exhibit significantly different electronic structures and physical behavior despite the similarity in their donor lattices, is now easy to understand. It is the result of the looser nature of the anion sheets in the latter. This looseness has two effects in the donor lattice. The first is to allow for smaller interactions between the donor molecules. The effect in the c_2 interaction is specially important because it subtly changes the nature of the band structure. The effect in the p-type interactions leads to a weak semimetallic overlap and thus to a potentially unstable metal. The second is to allow for a greater mobility of the donor molecules. This provides an easy mechanism by which the band overlap and thus the metallic character can be destroyed.

Unlike all previous salts, α-(BEDT-TTF)$_2$IBr$_2$ [26] and α-(BEDT-TTF)$_4$PtBr$_6$ [27] are semiconducting [29, 30]. Although both salts have donor layers of the α type they are not exactly like those of α-(BEDT-TTF)$_2$MHg(XCN)$_4$ and α-(BEDT-TTF)$_2$I$_3$. The donor layer of α-(BEDT-TTF)$_4$PtBr$_6$ is shown in Figure 11a. There are two different chains (A and B) but only two symmetry inequivalent BEDT-TTF donors (I and II). The important difference with the previous α type salts is that the angle between the two axes of the donor layer is now significantly different from 90° (see Fig. 11a). This leads to different angles between the donors of different chains and thus to different intrachain (c-type) and interchain (p-type) interactions. In both crystal and electronic structure α-(BEDT-TTF)$_2$IBr$_2$ and α-(BEDT-TTF)$_4$PtBr$_6$ are very similar so that we only report our results for the later. The calculated band structure is shown in Figure 11b and the transfer integrals are reported in Table VI. As can be seen in Figure 11b there is no band gap between the third and the fourth band which rules out the possibility of a band gap semiconductor. The third and fourth bands are however very narrow so that intrasite repulsions should dominate over band dispersion and lead to a localized system [49]. This is in agreement with the reported magnetic properties of α-(BEDT-TTF)$_2$IBr$_2$ [48]. Those of α-(BEDT-TTF)$_4$PtBr$_6$ have not been reported

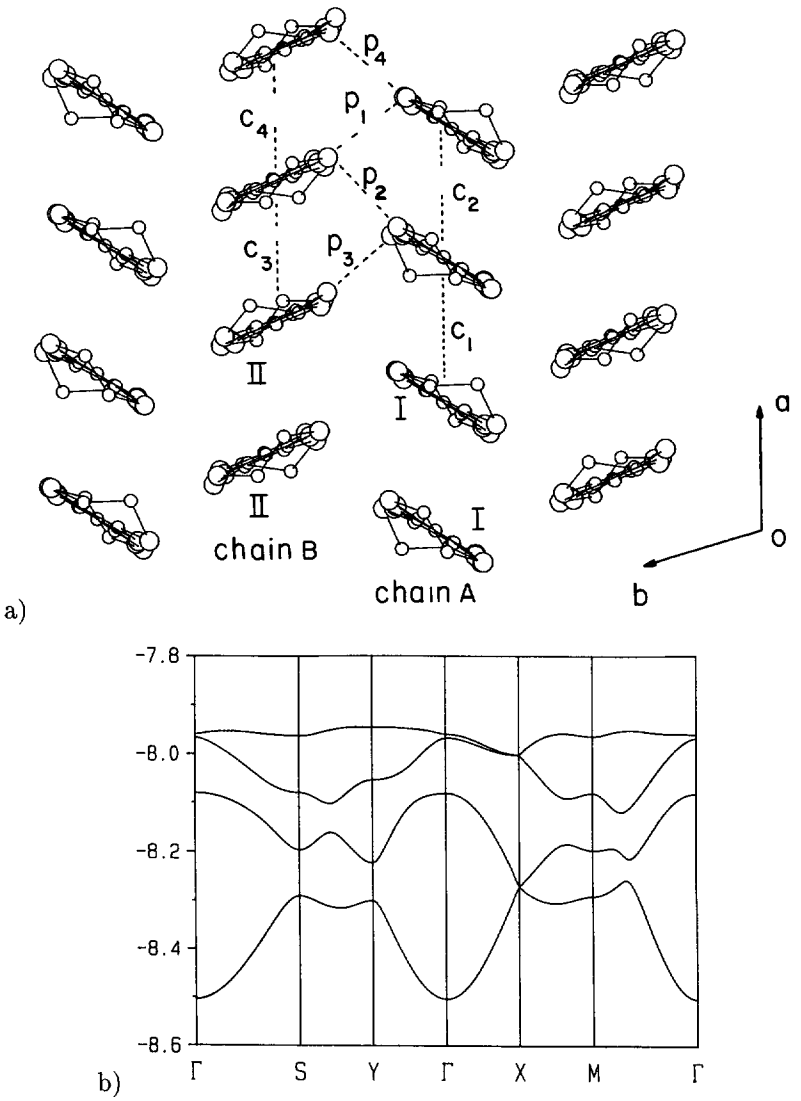

Fig. 11. — a) Perspective view of a donor layer of α-(BEDT-TTF)$_4$PtBr$_6$ where each molecule is viewed approximately along its central C = C bond and the hydrogen atoms are not shown for simplicity. b) Calculated dispersion relations for the HOMO bands of α-(BEDT-TTF)$_4$PtBr$_6$. Γ, X, Y, S, and M refer to the wave vectors (0, 0), ($a^*/2$, 0), (0, $b^*/2$), ($-a^*/2$, $b^*/2$) and ($a^*/2$, $b^*/2$), respectively. Energies are given in eV.

but we predict a similar behavior. As can be seen from Table VI, not only is c_2 very small but all the integrals are smaller than in the α-(BEDT-TTF)$_2$MHg(XCN)$_4$ phases. This fact makes this phase (as well as α-(BEDT-TTF)$_2$IBr$_2$) more similar to α-(BEDT-TTF)$_2$I$_3$ than to α-(BEDT-TTF)$_2$MHg(XCN)$_4$ but with even smaller interactions. The alternation of values of the transfer integrals along chains A and B suggest that the electrons of these lattices can be described as being localized in the dimers defined by interactions c_1 and c_4.

In summary, the nature of the anionic sheets seems to have a strong control of the stability of the metallic state of BEDT-TTF α phases. This control is exerted through different ways: first, by modulating the strength of the interchain (p-type) donor interactions; second, by controlling the easiness of the donor motions and third, by changing the strength of the c_2 interaction in the A donor chains. The stability of the metallic state of these phases results from a complex blend of these factors [50].

Acknowledgments

The authors are grateful to A.G. Khomenko and L.I. Buravov for the conductivity measurements as well as to M.V. Kartsovnik and V.N. Laukhin for fruitful discussions. This work was supported by the Russian Foundation for Fundamental Research (Grant 96-03-32029a), by the National Program of Russia on Advanced Problems of Physics of Condensed Matter (Project 93-030) and also partially by an INTAS Grant 93-2400. R. R. would like to thank the NSERC of Canada for a postgraduate research fellowship. E. C. would like to thank the CNRS for a sabbatical which made the stay at ICMAB possible.

References

[1] Oshima M., Mori H., Saito G. and Oshima K., *Chem. Lett.* (1989) 1159.
[2] Mori H., Tanaka S., Oshima M., Saito G., Mori T., Maruyama Y. and Inokuchi H., *Bull. Chem. Soc. Jpn* **63** (1990) 2183.
[3] Shibaeva R.P. and Rozenberg L.P., *Crystallogr. Rep.* **39** (1994) 47.
[4] Shibaeva R.P., Rozenberg L.P., Kushch N.D. and Yagubskii E.B., *Crystallogr. Rep.* **39** (1994) 747.
[5] Sasaki T., Toyota N., Tokumoto M., Kinoshita N. and Anzai H., *Solid State Commun.* **75** (1990) 93.
[6] Kinoshita N., Tokumoto M. and Anzai H., *J. Phys. Soc. Jpn* **60** (1991) 2131.
[7] Kushch N.D., Buravov L.V., Kartsovnik M.V., Laukhin V.N., Pesotskii S.I., Shibaeva R.P., Rozenberg L.P., Yagubskii E.B. and Zvarykina A.V., *Synth. Met.* **46** (1992) 271.
[8] Kartsovnik M.V., Kovalev A.E. and Kushch N.D., *J. Phys. I France* **3** (1993) 1187.
[9] Wang H.-H., Carlson K.D., Geiser U., Kwok W.K., Vashon M.D., Thompson J.E., Larsen N.F., McCabe G.D., Hulscher R.S. and Williams J.M., *Physica C* **166** (1990) 57.
[10] Schegolev A.I., Laukhin V.N., Khomenko A.G., Kartsovnik M.V., Shibaeva R.P., Rozenberg L.P. and Kovalev A.E., *J. Phys. I France* **2** (1992) 2123.
[11] Buravov L.V., Kushch N.D., Laukhin V.N., Khomenko A.G., Yagubskii E.B., Kartsovnik M.V., Kovalev A.E., Rozenberg L.P., Shibaeva R.P., Tanatar M.A., Yefanov V.S., Dyakin V.V. and Bondarenko V.A., *J. Phys. I France* **4** (1994) 441.
[12] Brooks J.S., Agosta C.C., Klepper S.J., Tokumoto M., Kinoshita N., Anzai H., Uji S., Aoki H., Perel A.S., Athas G.J. and Howe D.A., *Phys. Rev. Lett.* **69** (1992) 156.
[13] Klepper S.J., Brooks J.S., Chen X., Bradaric I., Tokumoto M., Kinoshita N., Tanaka Y. and Agosta C.C., *Phys. Rev. B* **48** (1993) 9913.
[14] Ducasse L., Fritsch A., *Solid State. Commun.* **91** (1994) 201.
[15] Osada T., Yagi R., Kagoshima S., Miura N., Oshima M. and Saito G., *Phys. Rev. B* **41** (1990) 5428.

[16] Pratt F.L., Singleton J., Doporto M., Fisher A.J., Janssen T.J.B.M., Perenboom J.A.A.J., Kurmoo M. and Day P., *Phys. Rev. B* **45** (1992) 13904.
[17] Wosnitza J., Crabtree G.W., Wang H.-H., Carlson K.D., Vashton M.D. and Williams J.M., *Phys. Rev. Lett.* **67** (1991) 263.
[18] Doporto M., Pratt F.L., Singleton J., Kurmoo M. and Hayes W., *Phys. Rev. Lett.* **69** (1992) 991.
[19] Sasaki T. and Toyota N., *Phys. Rev. B* **49** (1994) 10120.
[20] Kovalev A.E., Kartsovnik M.V. and Kushch N.D., *Solid State Commun.* **87** (1993) 705.
[21] Auban-Senzier P., Audouard A., Laukhin V.N., Rousseau R., Canadell E., Brossard L., Jérome D. and Kushch N.D., *J. Phys. I France* **5** (1995) 1301.
[22] Sasaki T., Ozawa H., Mori H., Tanaka S., Fukase T. and Toyota N., *J. Phys. Soc. Jpn*, submitted for publication.
[23] Bender K., Hennig I., Schweitzer D., Dietz K., Endres H. and Keller H.J., *Mol. Cryst. Liq. Cryst.* **108** (1984) 359.
[24] Shibaeva R.P., Kaminskii V.F. and Yagubskii E.B., *Mol. Cryst. Liq. Cryst.* **119** (1985) 361.
[25] Emge T.J., Leung P.C.W.L., Beno M.A., Wang H.-H., Williams J.M., Whangbo M.-H. and Evain M., *Mol. Cryst. Liq. Cryst.* **138** (1986) 393.
[26] Shibaeva R.P., Lobkovskaya R.M., Simonov M.A., Yagubskii E.B. and Ignat'ev A.A., *Sov. Phys. Crystallogr.* **31** (1986) 654.
[27] Shibaeva R.P. and Rozenberg L.P., *Sov. Phys. Crystallogr.* **35** (1990) 676.
[28] Dressel M., Gruner G., Pouget J.P., Breining A. and Schweitzer D., *J. Phys. I France* **4** (1994) 579.
[29] Galymzianov A.A., Ignatev A.A., Kushch N.D., Laukhin V.N., Makova M.K., Merzhanov V.A., Rozenberg L.P., Shibaeva R.P. and Yagubskii E.B., *Synth. Met.* **33** (1989) 81.
[30] Yagubskii E.B., Schegolev I.F., Shibaeva R.P., Fedutin D.N., Rozenberg L.P., Sogomonyan E.M., Lobkovskaya R.M., Laukhin V.N., Ignat'ev A.A., Zvarykina A.V. and Buravov L.I., *Pis'ma Zh. Eksp. Teor. Fiz.* **42** (1985) 167.
[31] Whangbo M.-H. and Hoffmann R., *J. Am. Chem. Soc.* **100** (1978) 6093.
[32] Ammeter J., Bürgi H.-B., Thibeault J. and Hoffmann R., *J. Am. Chem. Soc.* **100** (1978) 3686.
[33] Pénicaud A., Boubekeur K., Batail P., Canadell E., Auban-Senzier P. and Jérome D., *J. Am. Chem. Soc.* **115** (1993) 4101.
[34] Grant P.M., *J. Phys. Colloq France* **44** (1983) C3-847.
[35] Kobayashi H., Kobayashi A., Sasaki Y., Saito G. and Inokuchi H., *Bull. Chem. Soc. Jpn* **59** (1986) 301.
[36] Wells A.F., Structural Inorganic Chemistry (Oxford: Clarendon, 5th ed., 1984).
[37] Kinoshita N., Takahashi K., Murata K. and Anzai H., *Solid State Commun.* **67** (1988) 465.
[38] Kinoshita N., Tokumoto M., Murata K., Takahashi K., Anzai H., Mori T. and Honda K., *Synth. Met.* **41-43** (1991) 2107.
[39] Although the global topology of these Fermi surfaces is not strongly dependent on the computational aspects, fine details like the area or the warping of the 1D portion can depend. For instance the area does not only depend on the crystal structure but also on the radial extension of the Slater orbitals (see also Ref. [14]) as well as, even if to a lesser extent, on the mesh of k-points used to sample the Brillouin zone. The calculated areas of our Fermi surfaces are smaller than those obtained from magnetoresistance experiments (*i.e.*, 9-12% *vs.* 16% for the (S) salts). These values could have been easily adjusted to match the magnetoresistance results by slightly changing the Slater orbitals in our calculations.

Nevertheless, since our interest is on the comparison between the different salts and for reasons which will become clear later, we preferred to use exactly the same Slater orbitals as in all other studies of BEDT-TTF charge transfer salts previously performed in our group.

[40] Although the authors of references [2, 14] consider the existence of eight different types of donor···donor interactions, two of them (c_3 and c_4 in their reports) should be identical because of the existence of inversion centers in molecules II and III. The differences in the numerical values used for the corresponding transfer integrals in references [2, 14] should be due to some small numerical inaccuracy. It should also be pointed out that the labeling of interactions c_1 and c_2 in reference [14] is interchanged with respect to that used in reference [2] as well as in the present work.

[41] The calculated transfer integrals (eV) for the 104 K/298 K crystal structures are: $-0.012/-0.011$ (c_1), 0.140/0.125 (c_2), 0.074/0.074 (c_3), 0.129/0.113 (p_1), 0.116/0.100 (p_2), 0.162/0.156 (p_3) and 0.161/0.149 (p_4).

[42] Because of the similarity in the donor···donor interactions (*i.e.*, transfer integrals) the Fermi surfaces of the K(S) and K(Se) will be artificially similar if different HOMO energies (*i.e.*, site energies) for the I, II and III donors are not used in the model tight binding calculations. Although small differences in the HOMO levels usually do not lead to serious problems, one needs to be careful when the differences are not so small. This fact has already been recognized for a number of organic charge transfer salts. See for instance: Ducasse L., Abderrabba M., Gallois B. and Chasseau D., *Synth. Met.* **19** (1987) 327.

[43] Kovalev A.E., Kartsovnik M.V., Shibaeva R.P., Rozenberg L.P., Schegolev I.F. and Kushch N.D., *Solid State Commun.* **89** (1994) 575.

[44] Mori T., Kobayashi A., Sasaki Y., Kobayashi H., Saito G. and Inokuchi H., *Chem Lett.* (1984) 957.

[45] The calculated percentage changes in the absolute value of the transfer integrals when the temperature is lowered from 298 K to 120 K according to the structural data of reference [25] are: -44% (c_1), 19% (c_2), 63% (c_3), 40% (p_1), 3% (p_2), 10% (p_3) and 8% (p_4).

[46] A decrease in the absolute value of c_1 by 20% increases the band gap by about 50% and an increase of 20% in that of c_2 increases the band gap by about 60%.

[47] Endres H., Keller H.J., Swietlik R., Schweitzer D., Angermund K. and Krüger C., *Z. Naturforsch.* **41a** (1986) 1319.

[48] Nogami Y., Kagoshima S., Sugano T. and Saito G., *Synth. Met.* **16** (1986) 367.

[49] Here it should be pointed out that although the third and fourth bands of $\alpha-(\mathrm{BEDT-TTF})_2\mathrm{I}_3$ also look quite narrow, they acquire dispersion inside the Brillouin zone (along lines not shown in Fig. 10) leading to the practical disappearance of the gap. The total width of these two bands is around twice that of $\alpha-(\mathrm{BEDT-TTF})_2\mathrm{PtBr}_6$.

[50] After submission of this work a related paper dealing with the changes in the electronic structure of the $\alpha-(\mathrm{BEDT-TTF})_2\mathrm{KHg(XCN)}_4$) salt under pressure has appeared: Campos C.S., Sandhu P.S., Brooks J.S. and Ziman T., *Phys. Rev. B* **53** (1996) 12725. Although the approaches in the two papers are slightly different, the main results concerning the effect of pressure on the area of the closed part of the Fermi surface are similar.